UHasselt Computational Mathematics Preprint Series

Fractal structures in freezing brine

Sergey Alyaev, Eirik Keilegavlen, Jan Martin Nordbotten, Iuliu Sorin Pop

UHasselt Computational Mathematics Preprint Nr. UP-16-03

October 10, 2016

Fractal structures in freezing brine

Sergey Alyaev[12] Eirik Keilegavlen[1],†, Jan Martin Nordbotten[13] Iuliu Sorin Pop[41]

[1]Department of Mathematics, University Of Bergen, Postboks 7803, N-5020 Bergen, Norway

[2]International Research Institute of Stavanger, IRIS, Thormoehlensgt. 55, 5008 Bergen, Norway

[3]Department of Civil and Environmental Engineering, Princeton University, Princeton NJ08544, USA

[4]Faculty of Sciences, University of Hasselt, Campus Diepenbeek, Agoralaan building D, BE3590 Diepenbeek, Belgium

(Received xx; revised xx; accepted xx)

The process of initial ice formation in brine is a highly complex problem. In this paper, we propose a mathematical model that captures the dynamics of nucleation and development of ice inclusions in brine. The primary emphasis is on the interaction between ice growth and salt diffusion, subject to external forcing provided by temperature. Within this setting, two freezing regimes are identified, depending on the rate of change of the temperature: a slow freezing regime where a continuous ice domain is formed, and a fast freezing regime where recurrent nucleation appears within the fluid domain. The second regime is of primary interest, as it leads to fractal-like ice structures.

We analyse the critical threshold between the slow and fast regimes, by identifying the explicit rates of external temperature control that lead to self-similar salt concentration profiles in the fluid domains. Subsequent heuristic analysis provides estimates of the characteristic length scales of the fluid domains depending on the time-variation of the temperature. The analysis is sustained by numerical simulations.

Key words:

---

† Email address for correspondence: eirik.keilegavlen@uib.no

1. Introduction

Sea-ice represents an important component of the Arctic and Antarctic ecosystems, and forms the habitat for many micro-organisms. Of particular relevance are micro algae, which have high impact on heat and CO_2 exchange between the ocean and atmosphere (Büttner 2011; Thoms *et al.* 2014; Holland 2013). Having a different reflection coefficient (albedo) when compared to the ocean water, sea ice furthermore provides a feedback mechanism within global climate models (Hunke *et al.* 2011; Holland 2013).

The yearly cycle of the of sea-ice contains different phases: initial growth, salt rejection, and melting (Allison *et al.* 1985; Eicken 2003; Hunke *et al.* 2011). The processes of salt rejection and melting has been studied extensively in laboratory settings Eide & Martin (1975); Allison *et al.* (1985); Worster (1992); Eicken (2003); Vancoppenolle *et al.* (2006); Peppin *et al.* (2007); Hunke *et al.* (2011); Wells *et al.* (2011). These experimental studies provide the basis for the heuristic relationships required when developing computational models, which in their turn are needed for understanding large-scale dynamics. In contrast to this, studying the initial formation of the sea-ice in natural conditions is non-trivial, as taking field samples is a complex and even dangerous process (Büttner 2011).

This paper is concerned with mathematical modeling of ice formation in brine. In particular, the phase transition and the micro-scale diffusion of salt are explicitly accounted for, however, under idealized conditions: the temperature is constant in space and the fluid is stagnant within the domain. In one and two spatial dimensions (1D/2D), this is analogous to a column or a thin slit experiments.

The present work is complimentary to the classic work in Mullins & Sekerka (1964) on the stability of an advancing front of ice. Their analysisis inherently multidimensional and provides the conditions for an unstable evolution of the front. Our analysis is not focused on the stability of the front itself, but rather on the potential for spontaneous nucleation and growth of pre-frontal ice. To the best of our knowledge, there are no direct laboratory experiments considering this processes, but solidification effects ahead of the solid front in an analogous system has been observed experimentally in (Peppin *et al.* 2008).

Our analysis demonstrates that the interplay between the salt expulsions from the ice and the salt diffusion within the fluid can lead to complex structures. In particular, we identify cooling rates which allow for two types of self-similar freezing regimes: a trivial regime with compact ice growth, and a non-trivial one where the ice growth forms emerging fractal patterns. These fractal ice structures give insight into the transition between the liquid and the solid phase and therefore supplements the traditional, averaged mushy-layer approaches (Worster 1997; Hunke *et al.* 2011).

In addition to identifying self-similar structures for the freezing problem, we also derive an estimate for characteristic fluid-region length-scales, for general freezing regimes. Both fractal forming behavior and the robustness of fractal patterns with respect to perturbation of the initial conditions are verified numerically.

The structure of the manuscript is as follows. In section 2 we present the mathematical model for the sea-ice dynamics and identify the descriptive parameter, the Sherwood number. In section 3 we identify two regimes for the sea-ice formation and use a 1D model to derive the necessary conditions for sub-critical (compact) ice growth, respectively for super-critical (fractal) ice formation. Section 4 bridges the gap between the two regimes and presents an approximate semi-analytical algorithm that can be employed for characterizing the structure and distribution of the ice and brine regions formed inside the sea-ice region depending on the temperature evolution. Section 5 verifies the analysis

by comparison to numerical simulations of the governing model equations. Section 6 provides the conclusions.

2. The mathematical model

We consider the formation of ice in brine (salt water) with salinity u. Ice is formed due to the temperature decay, which is assumed constant in space and monotonic in time. The brine and ice together occupy the bounded domain G, consisting of two parts, the brine sub-domain Ω and the ice sub-domain $G\backslash\bar{\Omega}$, where $\bar{\Omega}$ stands for the closure of Ω. As will be explained below, the two sub-domains are evolving in time, depending on the a-priori unknown salinity u. Therefore on has $\Omega = \Omega(t)$, with $t > 0$ being the time variable. Although the analysis in later sections is carried for one spatial dimension, and thus G is a bounded, open interval in $\mathbb{R}$, the presentation of the mathematical model is kept general and remains applicable for general dimensions. Note however that we do not advective motion (in either the fluid nor the ice), and hence the model has greatest physical relevance when the fluid is essentially stagnant.

We assume that the concentration of salt in ice is constant, and without loss of generality we normalize this constant to zero:

$$u(t,x) = 0, \text{ for all } t \geqslant 0 \text{ and } x \notin \Omega(t). \tag{2.1}$$

Since Ω is time dependent, the brine-ice interface also evolves in time, and one has $\partial\Omega = \partial\Omega(t)$. In mathematical terms, $\partial\Omega$ is a boundary that moves freely inside G. The resulting is a a Stefan-type model (Voller *et al.* 2004; van Noorden & Pop 2007; Bringedal *et al.* 2015) that is capable to capture the complex geometry of the ice domain. This is alternative to the approach where space averaged mushy-layers are adopted for the small-scale mixture of ice and brine (Worster 1992, 1997; Petrich *et al.* 2004; Kutschan *et al.* 2010; Hunke *et al.* 2011).

The evolution of the salinity and the two phases, brine and ice, is governed by standard conservation laws (see e.g. Petrich *et al.* (2004); Katz & Worster (2008); Peppin *et al.* (2008)). For simplicity we assume that the energy is equilibrated instantaneously over the space, meaning that the temperature is constant in the ice-water domain G. This assumption is natural for 1D and 2D geometries (pipes and slits), where the external temperature controls the system directly. In 3D, this assumption requires thermal conduction to be sufficiently large relative to diffusion. With this assumption of constant temperature, we are allowed to replace the energy conservation equation by an algebraic relation between the critical salinity and the freezing temperature of the brine. In this respect we refer to Worster (1992); Katz & Worster (2008)), where this relation is provided as a phase diagram. As mentioned before, we assume that brine and ice coexist as distinct phases in the domain G, whereas salt only appears as a dissolved component in brine.

Further, instead of considering an up-scaled model involving averaged quantities like salt or brine volume ratio, the starting point here is at the scale where sharp interfaces separating the two phases can be identified. As mentioned before, these interfaces are evolving in time in a a-priori unknown manner and are therefore free boundaries. Since salinity is the controlling variable for freezing, the salinity of brine at the brine-ice interface equals the temperature-dependent critical salinity:

$$u(t,x) = u_{crit}(T(t)) = u_{crit}(t) \text{ for } t \geqslant 0,\ x \in \partial\Omega(t). \tag{2.2}$$

This is equivalent to saying that the freezing/melting temperature of the brine depends on the salinity. The temperature is the underlying control mechanism allowing to distinguish

between various ice formation regimes. Recalling the assumption made above on the instantaneous energy equilibration, the temperature enters in the system only through the critical salinity and plays further no explicit role in the present simplified model. Therefore in what follows T will be replaced by u_{crit} as the control mechanism. This is justified from physical point of view, as in general u_{crit} is a decreasing function of the temperature and thus a one-to-one relationship can be defined between the two quantities.

2.1. *Mass balance for salt*

The strong form of the salt mass balance equation is

$$\frac{\partial}{\partial t}u(t,x) = -\nabla \cdot \vec{J}_u \ , \text{ for } t \geqslant 0,\ x \in \Omega(t), \tag{2.3}$$

where $\vec{J}_u$ is the flux vector. Similar to Kutschan *et al.* (2010); Thoms *et al.* (2014), we neglect the expansion effects due to phase change and assume further that the fluid is at rest. As with the spatially isothermal assumption, this simplification can be justified strongly in 1D and 2D for pipes and slits, but requires further justifications in 3D. With diffusion is Fickian, the salt flux thus takes the form

$$\vec{J}_u\ (t,x) = -D\nabla u(t,x), \text{ for } t \geqslant 0,\ x \in \Omega(t), \tag{2.4}$$

where D is the diffusion coefficient, here taken as a constant. With this, the equation (2.3) becomes

$$\frac{\partial}{\partial t}u(t,x) = D\Delta u(t,x), \text{ for } t \geqslant 0,\ x \in \Omega(t). \tag{2.5}$$

2.2. *Salt expulsion at the boundary*

Since the ice is assumed salt-free, salt is expelled from the ice formed at the brine-ice interfaces. In order to conserve mass at the brine-ice interface the normal component of the salt expulsion flux $\vec{J}_{bc} \cdot \vec{n}$ and normal component of the diffusive flux $\vec{J}_u$ must equal

$$-\ \vec{J}_{bc} \cdot \vec{n} + \ \vec{J}_u \cdot \vec{n} = 0, \text{ for } t \geqslant 0 \text{ and } x \in \partial\Omega(t). \tag{2.6}$$

Here $\vec{n}$ is the normal vector at the boundary $\partial\Omega$ pointing inside the fluid. Letting $\vec{s}$ denote the position of the ice boundary, the conservation of salt as seen from the ice domain implies that the expulsion flux is given by

$$\vec{J}_{bc} \equiv u_{crit}\frac{d\vec{s}}{dt} \tag{2.7}$$

Together, equations (2.6) and (2.7) becomes a Rankine-Hugoniot condition at the brine-ice boundary

$$-u_{crit}\frac{d\vec{s}}{dt} \cdot \vec{n} + \vec{J}_u \cdot \vec{n} = 0, \text{ for } t \geqslant 0 \text{ and } x \in \partial\Omega(t). \tag{2.8}$$

Figure 1 is a one-dimensional illustration of the advancement ds of the ice-water boundary over an infinitesimal time dt, due to the increase of the critical salinity at the boundary from u_{crit} to $u_{crit} + du_{crit}$. This results in the salt expulsion flux J_{bc} at the boundary and the corresponding change in the overall salt profile from solid to dashed line as a result of the diffusion in the water domain.

2.3. *Nucleation*

Salinity and phase transition are two processes that are strongly connected. As seen from the discussion above, a decrease in the temperature can lead to freezing associated

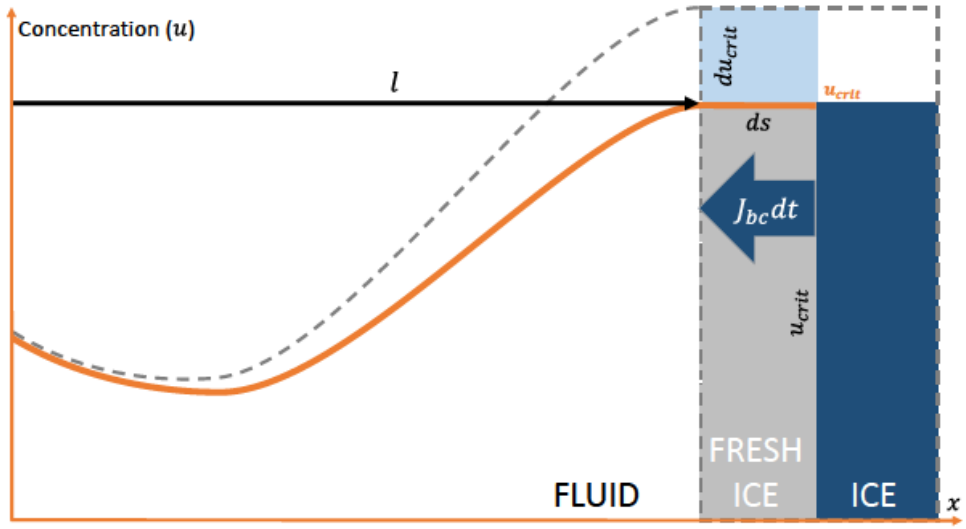

FIGURE 1. A sketch of the ice-water boundary movement caused by an increase of the critical salinity during freezing.

with exisiting ice regions through an increase of the critical salinity u_{crit}. A second important mechanism is the nucleation of new ice regions. While the exact laws of nucleation are difficult to obtain, we expect some supercooling to occur in the system, and thus here we consider nucleation to happen only when below a (salinity dependent) nucleation temperature. Conversely, this can be stated that nucleation only happens below a (temperature dependent) nucleation salinity. To be consistent with the treatment of freezing, we adopt this latter viewpoint, and thus we write $u_{nucl} = u_{nucl}(T(t)) = u_{nucl}(t)$. We will only consider the case where the nucleation salinity and the critical salinity are linearly related,

$$u_{nucl}(t) = \mu u_{crit}(t), \tag{2.9}$$

where $0 \leqslant \mu < 1$ is a constant nucleation multiplier. Once nucleation is encountered, salinity decreases locally due to ice formation (as discussed above), and a measurable region of ice is being formed at nucleation sites.

2.4. *The complete mathematical model*

In the continuation, we will always consider space, time and concentration dimensionless, in the sense that we use the natural non-dimensionalizations $x/x_* \to x$, $u_{crit}(t)/u_{crit}(0) \to u_{crit}(t)$ and $tD/u_{crit}(0) \to t$. Here x_* is the diameter of the domain (length, in 1D). Note that this implies that non-dimensionalised $u_{crit}(0) = 1$, and that the constant D is subsumed by the time derivatives in the equations.

The mathematical model discussed so far has the salinity u and the location of the ice-brine boundary $\partial\Omega$ as unknowns. The process is governed by the critical salinity at the ice-brine interface u_{crit}, which is temperature and thus time dependent, and defines the boundary conditions at $\partial\Omega(t)$.

$$\begin{cases} \frac{\partial}{\partial t}u(t,x) &= \Delta u(t,x), & \text{for } t \geqslant 0 \text{ and } x \in \Omega;; \\ u(t,x) &\geqslant u_{nucl}(t) & \text{for } t \geqslant 0 \text{ and } x \in \Omega; \\ u(t,x) &= 0 & \text{for } t \geqslant 0 \text{ and } x \notin \Omega; \\ u_{crit}(t)\frac{d}{dt}\vec{s}(t)\cdot\vec{n} &= (-\nabla u(t,x))\cdot\vec{n}, & \text{for } t \geqslant 0 \text{ and } x \in \partial\Omega; \\ u(t,x) &= u_{crit}(t) & \text{for } t \geqslant 0 \text{ and } x \in \partial\Omega. \\ u_{nucl}(t) &= \mu u_{crit}(t), & \text{for } t \geqslant 0. \end{cases} \tag{2.10}$$

The system is completed by initial conditions.

2.5. *Sherwood number*

In the absence of spontaneous nucleation, the qualitative behavior of the ice-water system can be characterized by a relation between the rate of the normal components of two fluxes at the moving ice-brine boundary: the salt expulsion flux (2.7) and the diffusive flux (2.4). We let ℓ be a time-dependent characteristic domain size that can be seen as an average distance between ice boundaries. Observe that the entire process considered here is controlled by the critical salinity u_{crit}, and this can change rapidly in time, inducing different sea ice formation regimes. Consequently, the characteristic domain size ℓ may change significantly in time.

We interpret K as a characteristic normal velocity of the ice-brine boundary (to be defined precisely below), which scales as

$$K \sim \frac{d\vec{s}}{dt} \cdot \vec{n}. \tag{2.11}$$

The ratio of mass transfer rate to the diffusion rate is essential for this problem, and is characterized by the Sherwood number (Cussler 2009), defined as (recall that the non-dimensionalized diffusion constant is unity):

$$\mathrm{Sh} = \frac{K}{\ell^{-1}}. \tag{2.12}$$

We emphasize that Sh may be variable in time as it depends on both ℓ and K, thus it is in principle a function. By a slight abuse of language, we will nevertheless refer to Sh as a "number". The case where Sh is constant in time will be of particular importance later.

To make concrete the choice of K, recall that the evolution of the ice-water interface is not known a-priori but represents an unknowns in the model. This evolution is controlled by u_{crit}, which is a time dependent input parameter of the model. As mentioned, K itself depends on time through ℓ, which on its turn depends on u_{crit}. Therefore it makes sense to express K in terms of the critical salinity. To do so we first refer to figure 1 sketching the change in the ice-brine system encountered within an infinitesimal time dt. More exactly, as suggested by the area of fresh ice, in the normal direction the ice front is moving into the brine over the distance $d\vec{s} \cdot \vec{n}$, causing a salt expulsion into the brine. The corresponding normal salt flux $\vec{J}_{bc} \cdot \vec{n} dt$ can be obtained from (2.7). Consequently, the salt is distributed into the brine domain sized ℓ (the left part of 1), causing an increase in the salinity by du_{crit} (the gray dashed curve). By mass conservation, one gets

$$\vec{J}_{bc} \cdot \vec{n} dt = u_{crit} d\vec{s} \cdot \vec{n} \sim \ell \left(\frac{d}{dt} u_{crit} \right) dt. \tag{2.13}$$

Dividing in the above by $u_{crit} dt$, from (2.11) we obtain the definition of the characteristic velocity of the system

$$K = \frac{\ell}{u_{crit}} \frac{d}{dt} u_{crit} = \ell \frac{d}{dt} \ln u_{crit}.$$

Combining the definition of the characteristic normal velocity with the Sherwood number in (2.12), we obtain

$$\mathrm{Sh} = \ell^2 \frac{d}{dt} \ln u_{crit}. \tag{2.14}$$

The Sherwood number as defined above will play a critical role in our subsequent analysis.

In addition to the Sherwood number, the model under discussion is also influenced

by the nucleation threshold. This is accounted for through the nucleation multiplier μ defined by equation (2.9), which is already a dimensionless parameter. In section 4 we show that the qualitative behavior of the system can be characterized based exclusively on two dimensionless parameters: the Sherwood number Sh and the nucleation multiplier μ.

2.6. *The dimensionless variables in 1D*

While the mathematical model defined above is stated for arbitrary dimensions, the analysis in the remainder of this manuscript is restricted to the case of one spatial dimension. For concreteness, we reformulate the variables of (2.10) accordingly, by employing the characteristic quantities discussed in section 2.5.

Now note that the freezing and nucleation given in (2.10) ensures that for the salinity u one has

$$\mu u_{crit}(t) \leqslant u \leqslant u_{crit}(t),$$

for any $t > 0$ and x in the brine domain. It therefore makes sense to introduce a time-dependent normalization by the salinity u_{crit}, such that the dimensionless salinity is constrained to the time-independent interval $(\mu, 1]$.

Furthermore, since the brine domain is a union of sub-intervals, we fix $t > 0$ and for any brine interval we let $x_0(t)$ denote its left boundary and $\ell(t)$ its length. This allows rescaling the spatial coordinate x by considering

$$y = (x - x_0(t))/\ell(t). \tag{2.15}$$

This allows the solution to be defined on the unit interval $y \in [0, 1]$. Finally, with the dimensionless time variable $\tilde{t} = t/T_{ch}$ (as mentioned, T_{ch} is a characteristic time) we can define a dimensionless salinity ν through

$$\nu : [0, \infty) \times [0, 1] \to (\mu, 1], \quad \nu(\tilde{t}, y) = \nu(\tilde{t}, (x - x_0(\tilde{t}T_{ch}))/\ell(\tilde{t}T_{ch})) = \frac{u(t, x)}{u_{crit}(t)}. \tag{2.16}$$

To simplify the notation, from now on the time should be interpreted as dimensionless and therefore we use the notation t instead of $\tilde{t}$. Since in the dimensionless form $y = 0$ and $y = 1$ are ice/brine boundaries and due to the scaling of the salinity one has $\nu(0) = \nu(1) = 1$. Also, (2.9) guarantees that ν cannot decrease below μ. In other words, whenever the minimum of ν is close to μ,the system is close to nucleation.

3. Rapid freezing in 1D

In the simplified 1D setting we consider (without loss of generality) that initially the brine occupies the interval $\Omega(0) \equiv (0, \ell_0)$, and that ice is present at the both boundaries. This can be the result of an initial nucleation.

The evolution of the salinity in a brine interval during rapid freezing is exemplified in figure 2, where three typical salinity profiles are displayed. To be more precise, let the environmental temperature be decreasing and hence the ice front advances into the brine. As stated, the temperature decay is associated with an increase of the critical salinity, as given in equation (2.2). This process can be observed in figure 2, where the brine domain is shrinking in time. On the other hand, the diffusion is smearing out the oscillations and propagate the increase in the salinity at the boundary towards the center of the fluid domain.

In the first instance, if the freezing is rapid the salinity changes near the boundary are larger than the changes in the interior. This leads to salinity profiles taking maximal

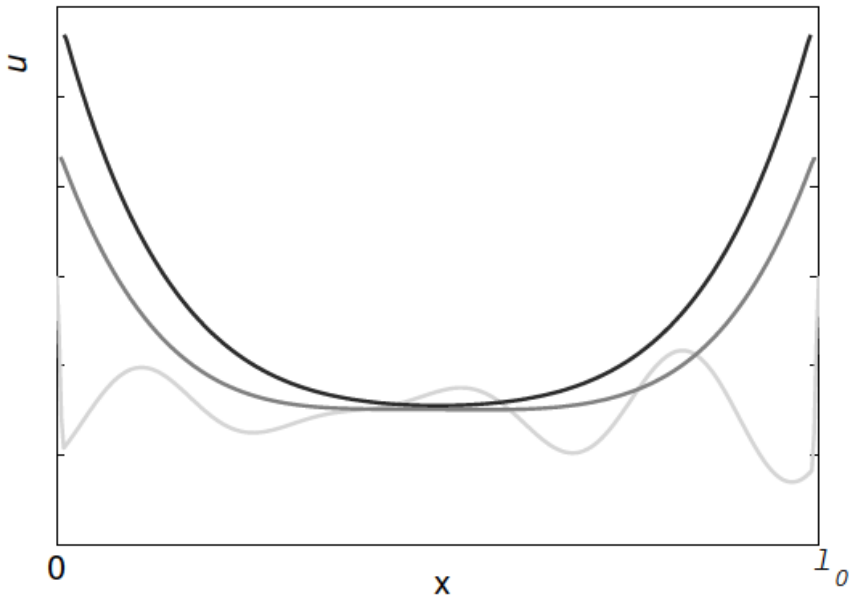

FIGURE 2. Salinity evolution in the fluid domain during rapid freezing (darker plots correspond to more recent times).

values equal to u_{crit} at the domain boundaries (the ice-brine interface) and lower ones in the middle of the fluid domain (see figure 2). In fact, the diffusion and the temperature decrease (or the increase of u_{crit}) are two effects that determine the behaviour of the system. Their interplay is characterized by the Sherwood number Sh discussed in section 2.5. In this context, three regimes can be identified, ordered by increasing Sherwood numbers:

(i) The *sub-critical regime*, when diffusion dominates and the solubility profiles are flattened out to u_{crit} and forming a continuous ice;

(ii) The *critical regime*, when diffusion balances the salinity changes due to temperature decrease, leading to self-similar solutions;

(iii) The *super-critical regime*, when the temperature decrease is dominating. In this case, the ratio between the minimum and the maximum values of the solubilities is decreasing until it reaches the nucleation multiplier defined in (2.9). At that point domain is split in two and the process continues in each sub-domain. If this process continues infinitely it will result in a Cantor-like set of sub-domains.

Since the Sherwood number is in principle changing in time, the system can switch from sub-critical to super-critical regimes and vice versa. The critical regime is the transition between the two regimes of compact and fractal ice growth. In the remaining of this section we derive the specific temporal control of u_{crit} that maintains the system in the critical regime.

3.1. *The critical case*

We define the critical case to be the state where the salinity profile is self-similar, and thus represents a case where no nucleation events occur. In other words, diffusion is in balance with the temperature decrease, representing a bifurcation point for the system. Recall that in this case the dimensionless solution function ν, as defined in (2.16), is in this case constant in time

$$\frac{\partial \nu(t,y)}{\partial t} = 0. \tag{3.1}$$

To simplify notation, since ν does not depend on, in this part we use the notation

$$\nu_1(y) \equiv \nu(t, y). \tag{3.2}$$

To find the boundary conditions leading to the critical case we consider ν_1 as a self-similar solution of the original problem, in the spirit of (Barenblatt 1996). Using (2.15) and (2.5) together with the chain rule, we obtain

$$0 = \frac{\partial \nu_1(y)}{\partial t} \equiv \frac{\partial \nu(t,y)}{\partial t} = \frac{1}{u_{crit}^2}\left[\frac{\partial u(t,x)}{\partial t} u_{crit} - \frac{du_{crit}(t)}{dt} u\right] \tag{3.3}$$

$$= \frac{1}{u_{crit}^2}\left[\frac{\partial^2 u(t,x)}{\partial x^2} u_{crit}(t) - \frac{du_{crit}(t)}{dt} u(t,x)\right] \tag{3.4}$$

$$= \frac{1}{\ell^2(t)} \frac{\partial^2 \nu_1(y)}{\partial y^2} - \frac{1}{u_{crit}(t)} \frac{du_{crit}(t)}{dt} \nu_1(y). \tag{3.5}$$

This expression, together with the definition of the Sherwood number given in equation (2.14) provides the equation for the self-similar solution ν_1:

$$\ell^2(t) \frac{d}{dt} \ln u_{crit}(t) = \mathrm{Sh} = \frac{\partial^2 \nu_1(y)}{\partial y^2} \frac{1}{\nu_1(y)}. \tag{3.6}$$

Since the self-similar solution ν_1 does not include an explicit time-dependency, we make the critical observation that for the critical case, the Sherwood number is constant. Thus equation (3.6) provides two results. First, it is the ordinary differential equation for the boundary salinity u_{crit} leading to a constant Sherwood number. Secondly, it is an equation providing the self-similar solution ν_1 for this external control.

3.1.1. *The external control required for the critical case*

We start with interpreting equation (3.6) in terms of u_{crit}. Observe that it involves two unknowns, u_{crit} and ℓ. These unknowns are related by mass conservation of salt in the whole fluid domain, as there is no nucleation events.

In other words, mass conservation for salt gives us

$$\frac{d}{dt} \int_{x_0(t)}^{x_0(t)+\ell_0(t)} u(t,x) dx = 0 \tag{3.7}$$

Using the definition of ν_1 and transforming the above to the domain $[0, 1]$ yields

$$\frac{d}{dt}\left[\ell(t) u_{crit}(t) \int_0^1 \nu_1(y) dy\right] = 0. \tag{3.8}$$

Since the integral is independent of time, we can conclude that the product of domain size and critical consentration is independent of time, i.e.

$$\ell(t) u_{crit}(t) = u_{crit,0} \ell_0 = 1 \tag{3.9}$$

Combining equations (3.6) and (3.9), we obtain

$$u_{crit}(t) = \left(1 - \frac{t}{t_\infty}\right)^{-\frac{1}{2}}. \tag{3.10}$$

where the integration constant is identified as the time before the brine salinity blows

up, which is related to the Sherwood number by

$$t_\infty = \frac{1}{2\mathrm{Sh}}. \tag{3.11}$$

We note that from equations (3.9) and (3.11) that the size of the brine region satisfies $\ell(t) = \left(1 - \frac{t}{t_\infty}\right)^{\frac{1}{2}}$. Thus consistent with the notion of mass conservation, as the salinity blows up when t approaches t_∞, the brine domain vanishes, $\ell(t_\infty) = 0$.

3.1.2. *The salinity in the critical case*

Wer now solve equation (3.6) to obtain ν_1 and from this the salinity. From the definition of ν in(2.16), the boundary conditions are

$$\nu_1(0) = \nu_1(1) = 1. \tag{3.12}$$

The solution to (3.6) satisfying these conditions is

$$\nu_1(y) = \frac{\cosh(\mathrm{Sh}^{\frac{1}{2}}(y - \frac{1}{2}))}{\cosh(\frac{1}{2}\mathrm{Sh}^{\frac{1}{2}})}, \tag{3.13}$$

where cosh is the hyperbolic cosine function. The equation (3.13) defines a family of solutions depending on the Sherwood number.

The above solutions are obtained in the absence of nucleation, in the sense that the constraint $\nu \geqslant \mu$ has not been enforced. The self-similar solution ν_1 has a minimum at $y = 1/2$, thus the nucleation threshold is given as

$$\nu_1(1/2) = \frac{1}{\cosh(\frac{1}{2}\mathrm{Sh}^{\frac{1}{2}})} > \mu. \tag{3.14}$$

Since the self-similar solution is not valid across nucleation events, we interpret inequality (3.14) as a constraint on admissible Sherwood numbers for the critical solution, i.e. the freezing must be sufficiently slow such that

$$\mathrm{Sh} \leqslant \left(2\mathrm{arcCosh}\frac{1}{\mu}\right)^2. \tag{3.15}$$

This bound on the Sherwood number is essential, as it defines the largest possible constant Sherwood number for this system. When inequality (3.15) is violated, nucleation will happen, and thus the length-scale ℓ will be reduced, thus also reducing the Sherwood number. Conversely, we can consider the equaity (3.15) as a characteristic property of nucleation events. We explore these concepts in the next section.

3.2. *The super-critical, fractal case*

The super-critical case appears when freezing dominates the diffusion. Due to this, a rapid increase of the critical salinity is encountered and ν, the ratio between the critical salinity and the minimal one, decreases to μ, when nucleation appears. For symmetry reasons, we expect that nucleation happens near the middle of a brine domain, we approximate the splitting of the domain into two equal parts - see figure 3. This leads to two domains of halved lengths and, by (2.14), to a decrease in the Sherwood number. A lower Sherwood number together with a steeper salinity gradient near the newly created boundaries, leads to a local diffusion-dominated solution profile until freezing starts to dominate again and the process repeats. Following this scenario, one may expect a fractal structure similar to a Cantor set for the fluid domain.

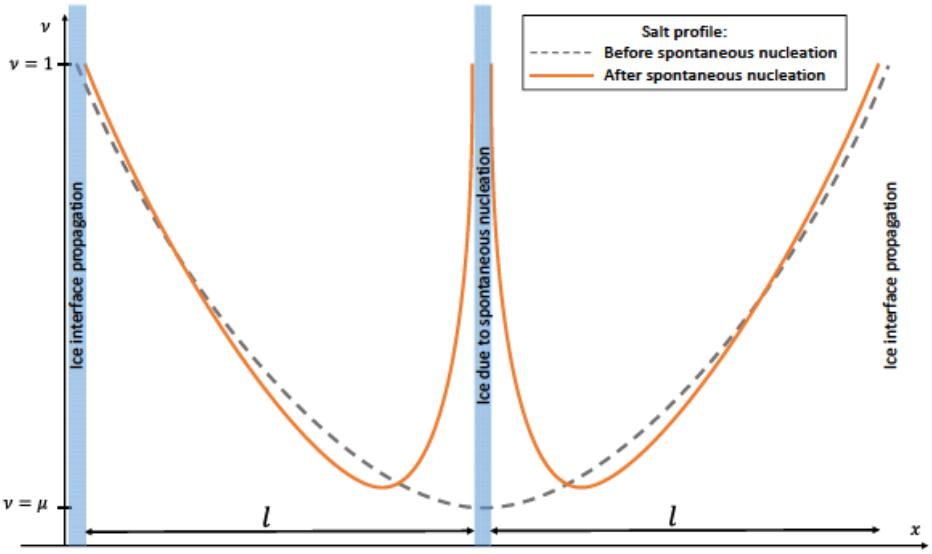

FIGURE 3. A schematic plot illustrating the change in the solution u due to spontaneous nucleation in the middle of the domain.

Following the approach of the critical case described in section 3.1, a self-similar solution is being sought. However, in this case nucleation and hence brine interval splitting, is encountered at certain times, which is the underlying mechanism to generate fractal solutions. We understand that the fractal case, we cannot have a constant Sherwood number, and thus that a freezing rate scaling as (3.10) will not be present. Indeed, in this section, we will show that for a different exponent in the control of the critical salinity, persistent nucleation can occur, and provide the connection between the control on the critical salinity and the relative freezing and nucleation processes.

As the domain splits into smaller sub-domains, the typical length scale becomes smaller, and the same should happen with the time scale characterizing the process between two nucleation events. To reflect this, a non-linear transformation of the time variable is introduced, with respect to which the dimensionless solution ν has a periodic behaviour in time

$$t = f(\eta). \tag{3.16}$$

The function f is a nonlinear, continuous and increasing transformation of time, which will be specified later. At the present we require that the transformation ensures that ν is periodic with period 1 in the transformed time variable η.

In the critical case discussed in section 3.1 the Sherwood number was constant in time. Here we use the ansatz that the Sherwood number has the same periodic structure as the domain, i.e. that it is one-periodic with respect to the time-variable η:

$$\mathrm{Sh}(\eta) = \mathrm{Sh}(\eta + 1), \tag{3.17}$$

In the super-critical case the brine domain Ω is complex, consisting of several sub-domains (intervals). Since the Sherwood number is no longer constant in the nucleation case, we introduce a new parameter to characterize the system in this regime. Thus let $\lambda > 1$ be a similarity parameter, such that between two nucleation events each interval decreases λ times as the ice boundaries propagate inwards. This non-dimensionless parameter thus gives the balance between freezing and nucleation, and in particular small values of λ close to 1 represent nucleation dominated, while large values of λ represent freezing dominated.

Denoting by again the nucleation moments by the time variable η taking integer values

i, this translates into

$$\ell((i+1)^-) = \frac{1}{\lambda}\ell(i^+). \tag{3.18}$$

The superscripts $\pm$ should be interpreted as the right and left limits. Further, once a spontaneous nucleation event is encountered in an interval each fluid sub-domain splits into two halves, thus $2\ell(i^+) = \ell(i^-)$ and the total decrease of the domain over one self-similarity period is given by (for all values of η)

$$\ell(\eta+1) = \frac{1}{2\lambda}\ell(\eta). \tag{3.19}$$

Additionally, we can express mass conservation of salt in the system as

$$n(\eta)\bar{\ell}(\eta)\bar{u}(\eta) = n(0)\bar{\ell}(0)\bar{u}(0) = \bar{u}(0) \tag{3.20}$$

Letting $\bar{u}(\eta) = \frac{1}{|\Omega(\eta)|}\int_\Omega(\eta)u(\eta,x)dx$ stand for the average salinity in the brine at time η. The quantity of $\bar{u}(\eta)$ is unknown, but can be approximate by $u_{crit}(\eta)$ to deduce the characteristic domain size

$$\bar{\ell}(\eta) = \frac{\bar{u}(0)}{n(\eta)u_{crit}(\eta)} \approx \frac{1}{n(\eta)u_{crit}(\eta)}. \tag{3.21}$$

We used earlier the integer i as a count of the number of nucleation times, and furthermore, will abuse slightly the notation by always interpreting i as the value of η rounded up to the nearest integer, i.e. $i = \lceil\eta\rceil$. Combining equations (3.19) and (3.21), we now obtain a direct expression for the dimensionless time, in terms of the new dimensionless parameter λ:

$$\ell(i^+) = \frac{1}{2^i}\frac{1}{u_{crit}(i)}. \tag{3.22}$$

Equation (3.19) gives

$$i = \frac{-\ln(\ell(i^+))}{\ln(2\lambda)}, \tag{3.23}$$

which, together with (3.22) leads to

$$\ell(i^+) = \exp\left(\frac{\ln(\ell(i^+)}{\ln(2\lambda)}\ln 2\right)\frac{1}{u_{crit}(i)} = \frac{\ell(i^+)^{1-\gamma}}{u_{crit}(i)}, \tag{3.24}$$

with the exponent

$$\gamma = \frac{\ln\lambda}{\ln 2\lambda}. \tag{3.25}$$

This exponent represents an essential scaling parameter of the super-critical case, and will appear throughout the following results. Note again that for large λ, we obtain $\gamma \approx 1$, and in particular recover the case from section 3.1.

From equation (3.24) we can now express ℓ as an explicit function of u_{crit}

$$\ell(i^+) = u_{crit}(i)^{-1/\gamma}, \tag{3.26}$$

Inserting the above into the definition of the Sherwood number, together with the ansatz (3.17) yields,

$$u_{crit}(i)^{-(1+2/\gamma)}\frac{d}{dt}u_{crit}(t) = \mathrm{Sh}(0^+) \tag{3.27}$$

at any time $t = f(i)$ when nucleation occurs.

It is natural to consider that the external control u_{crit} evolves continuously. As an

example we observe that equation (3.27), is satisfied by the following equation, similar in structure to (3.10)

$$u_{crit}(t) = \left(1 - \frac{t}{t_\infty}\right)^{-\frac{\gamma}{2}}. \tag{3.28}$$

As in the critical case, t_∞ is a time when the entire domain is completely frozen, which can be calculated analogously as before as

$$t_\infty = \frac{\gamma}{2\mathrm{Sh}(0^+)} \tag{3.29}$$

We close the section by noting that we can obtain an explicit expression for the non-linear time-transformation, by combining equations (3.23), (3.26) and (3.28), which gives the expression

$$t = f(\eta) = t_\infty \left[1 - (2\lambda)^{-2\eta}\right]. \tag{3.30}$$

Thus, we have identified the relationship between super-fast freezing (in the sense of equation (3.28) with $\gamma < 1$), and the relative importance of freezing and nucleation processes as characterized by λ.

4. Estimating the ice properties for general boundary conditions

Section 3 shows that the freezing and nucleation in brine can be understood for critical salinities $u_{crit}(t)$ changing on the form of equation (3.28). In general situations this critical salinity will not follow such temporal evolution, however we postulate that the qualitative behaviour during freezing, and in particular the partitioning of the domain, can be the same for a wider class of freezing rates. In this section we use the categorization of the Sherwood number as the critical parameter for unstable ice growth to obtain approximations for the characteristic length of the fluid/brine domain. In particular, we exploit the fact observed in section 3.1, that during nucleation, the Sherwood number can be approximated by equation (3.15).

As seen in section 3.1, nucleation leads to a split of a brine interval into two sub-intervals. To capture this binary behaviour we consider the class of functions

$$\mathbb{P}^{2,+} := \{f : [0,\infty) \to [0,\infty), f \text{ is non-decreasing and for all } k \in \mathbb{N}, f(k) = s^k\}$$

To be precise, we consider a given, monotone critical salinity $u_{crit}(t)$ and seek the integer function $n(t) \in \mathbb{P}^{2,+}$ and the real function $\bar{\ell}$ characterizing the number of brine regions and their characteristic length, respectively.

Recall the expression for the characteristic system length given in (3.21). This expression can be used with the definition of the Sherwood number, equation (2.14), to obtain the Sherwood number expressed in terms of the number of brine intervals

$$\mathrm{Sh}(t) = \frac{1}{n^2(t)u_{crit}^3(t)} \frac{du_{crit}(t)}{dt}. \tag{4.1}$$

As nucleation events occur, we know that the Sherwood number is well approximated by the equality in equation (3.15). Using this, we define $n^*(\cdot)$ as the continuous function obtained from the upper bound on Sh in the critical case

$$n^*(t) = \frac{\tilde{U}_0}{2}\left[\mathrm{arcCosh}\left(\frac{1}{\mu}\right)\right]^{-1}\left(\frac{1}{u_{crit}^3(t)}\frac{du_{crit}(t)}{dt}\right)^{\frac{1}{2}}. \tag{4.2}$$

Clearly, $n^*(t)$ is in general not be a natural number, and may be decreasing. To obtain a

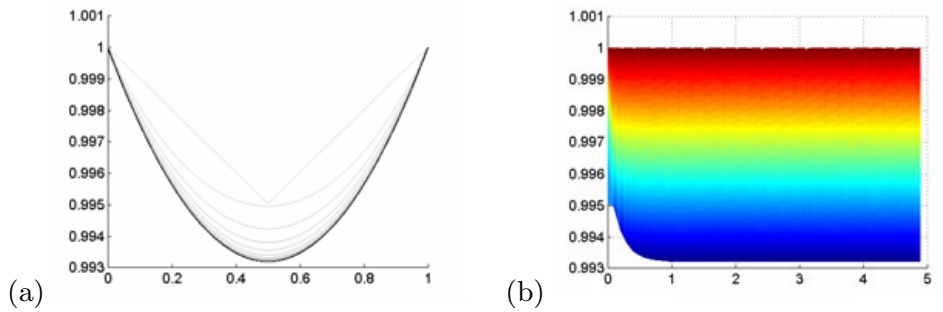

FIGURE 4. (a) The function ν at various times (darker color corresponding to later time); (b) the solution surface plotted against dimensionless time.

discrete number of fluid domains, for any $t > 0$ we take the maximum value (over time) of n^* rounded up, to obtain

$$n(t) = \max_{0 \leqslant \tau \leqslant t} \lceil n^*(\tau) \rceil_{\mathbb{P}^{2,+}}, \tag{4.3}$$

where $\lceil y \rceil_{\mathbb{P}^{2,+}}$ is the smallest integer power of 2 that is larger than y. By definition, $n(\cdot)$ is a function from $\mathbb{P}^{2,+}$. Moreover, for any t one has $n(t) \geqslant n^*(t)$, thus it is implied that freezing processes are excluded. From equations (4.3) and (3.21) we can also recover the characteristic length $\bar{\ell}$.

We emphasize on the fact that due to the approximation in equation (3.21), this derivation is not exact. Its accuracy depends on whether and how fast the solution approaches the self-similar structure assumed up to now. This aspect is investigated in the section 5.3.

5. Numerical examples

In this section we present numerical solutions to the system of equations (2.10), derived in the section 2.4. These solutions are computed by employing a cell-centered finite volume method, which is presented in detail in the appendix A.

We start with numerical experiments that investigate the regimes identified in the section 3. First, in the subsection 5.1 verify that the system converges to the self-similar solution identified in equation (3.13) for the critical case.. Secondly, we consider the super-critical regime, using the external control proposed in equation (3.28). Finally, we consider the verify the applicability of the discussed in section 4, both for an idealized case of external control provided by equation (3.28), as well as a more challenging case with a logistic funciton controlling the freezing process.

5.1. *Convergent solutions in the critical case*

We start by considering the self-similar salinity profile for the critical case derived in (3.10). Figure 4 presents the numerical results for the critical case. More precisely, it displays the scaled, dimensionless salinity ν introduced in (2.16). The initial condition in the numerical simulation is

$$\nu(x, 0) = 0.01 \cdot |x - .5| + .995, \text{ for } x \in [0, 1], \tag{5.1}$$

and the computation is for $\mathrm{Sh} = 0.5$ As seen in figure 4a, the numerical approximation eventually converges to the analytical solution (3.13).

Figure 4b presents the solution in $\eta \times \nu$ axes, see figure 4b. The lowest surface line in this projection illustrates the time evolution of $\frac{\min(u)}{\max(u)} = \min(\nu)$, that is, the quantity which

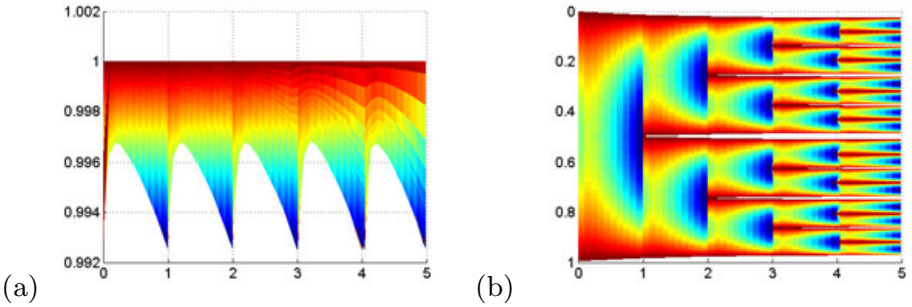

(a) (b)

FIGURE 5. Demonstration of the fractal forming behavior for the super-critical conditions given in equation (3.28). Figure (a). shows minimum concentration (lower bound) and concentration profiles (colors), while figure (b) shows the concentration (colors) plotted on the domains as they split, thus white represents ice. For both figures, time is given with respect to the transformed time η.

will trigger secondary nucleation if it drops below the nucleation multiplier μ defined in (2.9). Thus, the simulations reported here, are valid for any $\mu \leqslant 0.993$.

The convergence of the solution to the self-similar profile predicted by theory indicates that the self-similar solution ν is robust with respect to perturbations, an observation which is supported by other calculations not shown herein.

5.2. *The numerical validation of the fractal forming behavior*

The numerical experiments in this subsection verify that the condition for the external control on the critical salinity given in equation (3.28) indeed leads to binary, Cantor-set-type, fractals. This numerical approach particularly important since in the super-critical fractal case it is not feasible to obtain an explicit self-similar solution as for the critical case. For this example we use $\mathrm{Sh}(0+) = 0.02$, which is consistent with a nucleation threshold of 0.9925 according to inequality (3.15). The fractal formation is then characterized by the balance between freezing and nucleation, which we set to $\lambda = 1.03$.

The salinity profile immediately after nucleation events converges towards a (non-symmetric) self-similar solution after a few nucleation events, and thus the initial condition is immaterial for the asympotitc behavior of the system. To reflect this, we only show the solution after it has converged to the self-similar profile, typically within two-three splitting steps. We return to the pre-asymptotic regime in section 5.3.1.

The solution is shown in figure 5 for a time-span covering several nucleation events. As the numerical simulation evidences, each sub-domain splits into two equal sub-domains, and with the period 1 in the non-linear time η. This provides a *post hoc* justification of the assumptions stated in section 3.2.

The self-similarity of the solution implies that the process will continue as $\eta \to \infty$, leading to an countable infinity of splittings within finite time (recall that t_∞ is finite). This results in a bipartite tree of sub-domains that, at each time, is an approximation of a Cantor-like set.

5.3. *Applying the approximate method to determine the properties of the sea-ice*

In this subsection we show validate the heuristically derived Sherwood number Sh and mean brine-subdomain length-scale n derived in section 4. We use this opportunity to consider the pre-asympotic regime alluded to in the previous section.

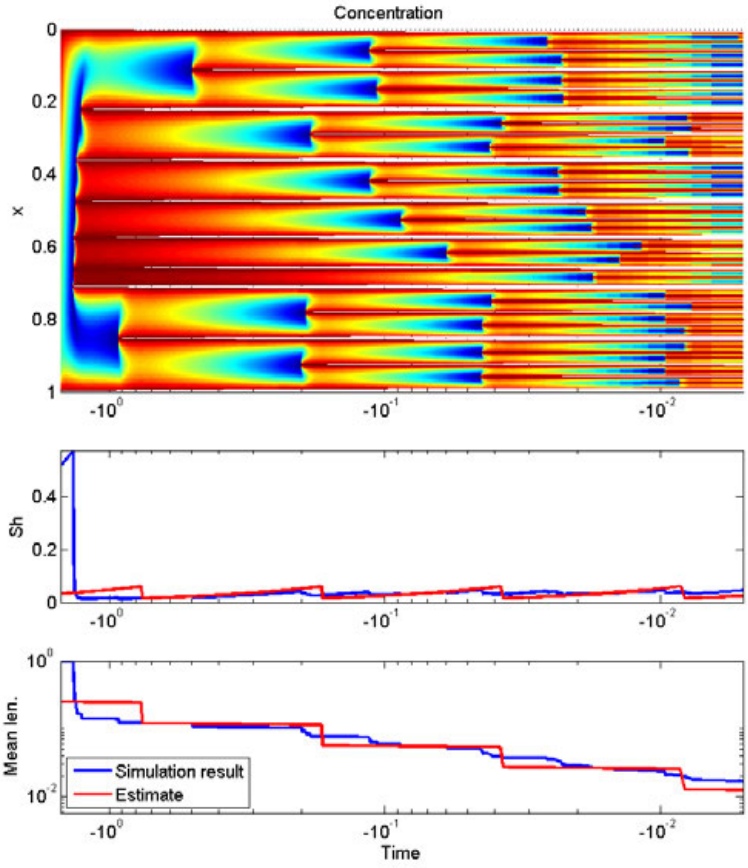

FIGURE 6. Comparison of simulated and estimated Sherwood number and average sub-domain size for a solution including the pre-asymptotic regime.

5.3.1. *Fractal solutions including the pre-asymptotic regime*

We consider an asymmetric initial condition leading to initial asymmetrical splitting, and thus the different brine sub-domains have different widths. In this case, the fractal does not have a pure binary structure anymore. This can be seen in figure 6, where each individual branch of the solution approaches an asymptotic regime after about four splittings. Note that for these figures, we choose to use dimensionless time t rather than η, and to better visualize the results, we use the logarithm of $t - t_\infty$ as the x-axis.

As the numerical solution is driven by a prescribed $u_{crit}(t)$, as detailed in section 5.2, we can apply the estimates for the mean length scale, as well as the Sherwood numbers, as given by equations (4.3) and (4.1). The estimates are compared against the true values obtained from the simulation in the lower part of figure 6. Since the estimate from section 4 does not know the initial salinity distribution, it cannot capture the details at the earliest stage of the simulation. However, for later times, we find a very reasonable agreement between the estimated and simulated values.

5.3.2. *A generic rapid freezing scenario*

As a final comparison, we consider a case of rapid freezing where the boundary salinity controlling the freezing process does not follow the monomial scaling give in equation (3.28). In particular, we consider the logistic function,

$$u_{crit}(t) = 1 + \frac{5}{(1 + \exp(10(-t + 1))}, \qquad \text{for } t \in [0, 1.5]. \tag{5.2}$$

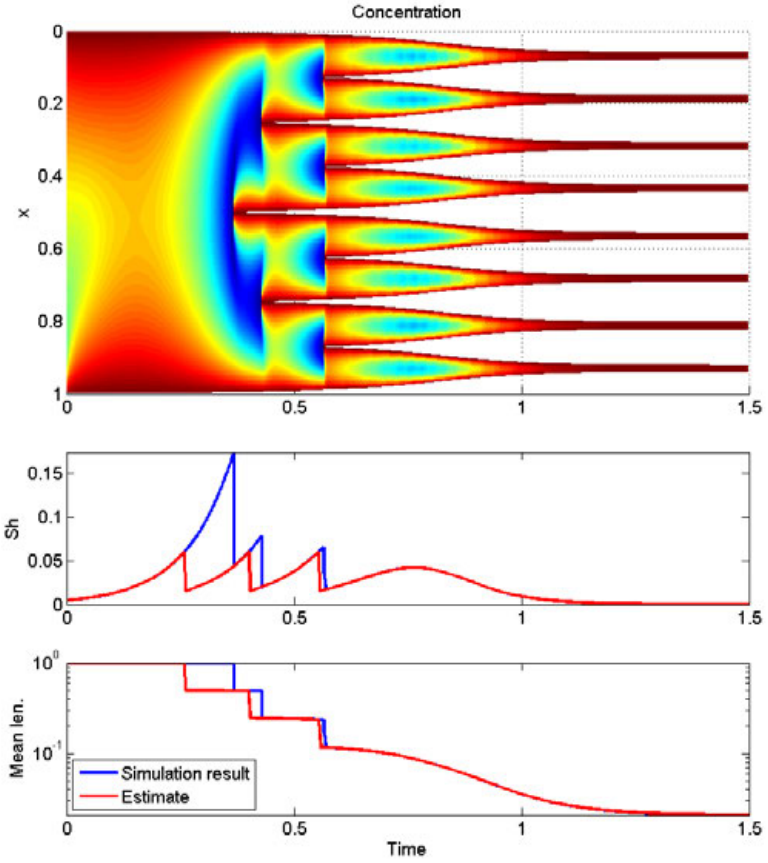

FIGURE 7. Comparison of simulated and estimated Sherwood number and average sub-domain size for a logistic function boundary conditions.

This choice is motivated by the transition from a slow, diffusion dominated, regime, via a nucleation dominated regime, and finally a diffusion dominated regime. We consider this a challenging test for the heuristic estimates derived in section 4.

The numerical solution and the comparison of the characteristic parameters are depicted on figure 7. We first note the rapid establishment of an asymptotic-like fractal structure, in the sense of the division of the original brine-domain into 8 nearly equisized partitions. This provides additional support to the applicability of the analysis of section 3 for general freezing regimes.

Secondly, we note from the lower figures that the estimates for characteristic brine-domain length and Sherwood number is in general very close to the computed values. Again the discrepancy is related to the salinity distribution at the onset of the freezing process, which is not captured, leading to a prediction of premature nucleation. As the nucleation process is established, the estimates approach the calculated values both of Sherwood number and of domain-size, with the correct prediction of 8 fluid domains. As expected, the heuristic algorithm gives a very close match for the final smooth regime (starting from $t \approx 0.7$) where the solution is close to the steady state.

6. Conclusions

In this paper we have presented a mathematical model for the ice-formation in brine. We avoid mushy-layer approximations, and formulate the model explicitly in terms of the phase change (ice-brine) encountered at the lowest continuum scale.

For the one-dimensional setting, we identify three freezing regimes: a sub-critical (slow) freezing regime where a continuous ice domain is formed, a critical regime when self-similar profiles are determined explicitly, and a super-critical (fast) freezing regime leading to fractal-like structures. A main contribution of the work is the explicit characterization of the critical regime, which the transition between solid and fractal freezing.

We exploit the characterization of the critical regime to both give a structural understanding of super-critical (nucleation-dominated) freezing, but also to derive closed-form estimates of characteristic ice-domain length-scales for the whole time-dependent freezing process. These latter estimates form the initial steps towards a more rigorous understanding of the link between freezing condition and physical parameters for the resulting porous structure.

A finite volume method is proposed for solving the moving boundary models posed at the smallest scale. This numerical approach is used to verify the exact solution obtained in the critical regime. Under the fractal behaviour conditions obtained in the super-critical regime, the numerical solution shows the expected nucleation process, approaching a Cantor-set-like fractal structure.

Acknowledgement SA thanks Anna Kvashchuk for useful discussions during preparation of the manuscript. JMN visited the Isaac Newton program "Melt in the Mantle" at Cambridge University while working on this manuscript. ISP acknowledges the support from the Akademia grant of Statoil and from the Research Foundation - Flanders FWO through the the Odysseus programme grant G0G1316N.

Appendix A

This appendix presents the numerical method used to solve the model equations at the scale of a single brine domain.

To obtain a numerical solution for the one-dimensional model in section 2 we have modified a standard finite volume method with an explicit Euler time stepping.

Due to the ice domains acting as barriers, the scheme only needs to account for a single brine domain - multiple domains are handled by recursively calling new instances of the scheme. It is therefore sufficient for the numerical method to handle a) diffusion of salt in the brine phase, b) motion of ice interfaces, and c) nucleation events. The diffusion of salt in the brine phase is standard, and will not be discussed further.

The motion of ice interfaces is necessary to resolve on a sub-grid scale. Thus, as indicated in figure 8, the ice domain is permitted to partially enter cells, and these cells thus have an internal variable indicating the salt content. It is important to note that the boundary cells have prescribed salt concentration, and it is imperative that the mass balance relations for diffusion out of the boundary cell is solved together with the propagation of the ice boundary. The scheme allows for the ice to completely fill a cell during a time-step, and continue into the neighboring cell.

Finally, a similar approach is taken for the nucleation events. In particular, the salt balance is again ensured strongly. Thus the nucleation event is associated with the formation of a non-zero amount of ice, which is calculated such that the expelled salt provides the correct critical salinity in the remaining parts of the cell(s) where the

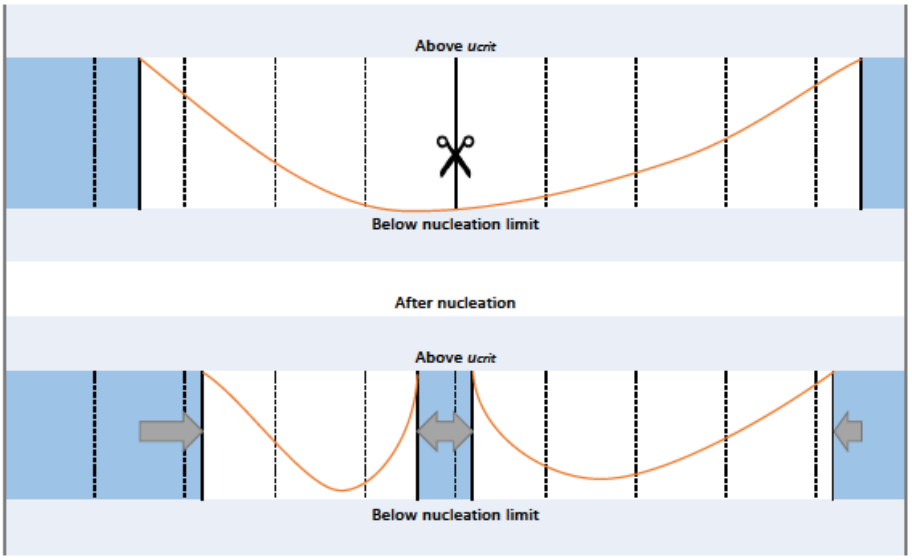

FIGURE 8. Cartoon illustrating the finite difference method, including the occurrence of spontaneous nucleation. Dashed lines represent the boundaries of the grid cells. The sub-domains occupied by the solid are filled, the scissors indicate the place where splitting occurs due to nucleation, the arrows show how the ice domain has expanded.

nucleation event occurs. After the new ice is calculated for the nucleation event, the domain is split into two independent calculations, and the grid is refined if necessary.

REFERENCES

ALLISON, IAN, TIVENDALE, C. M. & COPSON, G. R. 1985 Annual salt and energy budget beneath an antarctic fast ice cover. *Annals of Glaciology* (6).

BARENBLATT, GRIGORY ISAAKOVICH 1996 *Scaling, self-similarity, and intermediate asymptotics: dimensional analysis and intermediate asymptotics*, , vol. 14. Cambridge University Press.

BRINGEDAL, C., BERRE, I., POP, I. S. & RADU, F. A. 2015 A model for non-isothermal flow and mineral precipitation and dissolution in a thin strip. *J. Comput. Appl. Math.* **289**, 346–355.

BÜTTNER, JULIANE 2011 Permeability of young sea ice from microtomographic images. PhD thesis, University of Bergen.

CUSSLER, EDWARD LANSING 2009 *Diffusion: mass transfer in fluid systems*. Cambridge university press.

EICKEN, HAJO 2003 From the microscopic, to the macroscopic, to the regional scale: growth, microstructure and properties of sea ice. In *Sea ice: an introduction to its physics, chemistry and geology* (ed. David N. Thomas & Gerhard S. Dieckmann), pp. 22–81. London: Blackwell Science.

EIDE, L.I. & MARTIN, S. 1975 The Formation of Brine Drainage Features in young sea ice. *J. Glaciol* **14** (70).

HOLLAND, DAVID M. 2013 The marine cryosphere. *International Geophysics* **103**, 413–442.

HUNKE, E. C., NOTZ, D., TURNER, A. K. & VANCOPPENOLLE, M. 2011 The multiphase physics of sea ice: a review for model developers. *The Cryosphere* **5** (4), 989–1009.

KATZ, RICHARD F. & WORSTER, M. GRAE 2008 Simulation of directional solidification, thermochemical convection, and chimney formation in a Hele-Shaw cell. *Journal of Computational Physics* **227** (23), 9823–9840.

KUTSCHAN, B., MORAWETZ, K. & GEMMING, S. 2010 Modeling the morphogenesis of brine channels in sea ice. *Physical Review E* **81** (3), 036106.

MULLINS, W. W. & SEKERKA, R. F. 1964 Stability of a planar interface during solidification of a dilute binary alloy. *Journal of Applied Physics* **35** (2), 444–451, arXiv: arXiv:1011.1669v3.

VAN NOORDEN, T. L. & POP, I. S. 2007 A Stefan problem modelling crystal dissolution and precipitation. *IMA Journal of Applied Mathematics* **73** (2), 393–411.

Peppin, S. S. L., Aussillous, P., Huppert, Herbert E. & Worster, M. Grae 2007 Steady-state mushy layers: experiments and theory. *Journal of Fluid Mechanics* **570**, 69.

Peppin, S. S. L., Huppert, Herbert E. & Worster, M. Grae 2008 Steady-state solidification of aqueous ammonium chloride. *Journal of Fluid Mechanics* **599**, 465–476.

Petrich, Chris, Langhorne, PJ & Sun, Zhifa 2004 NUMERICAL SIMULATION OF SEA ICE GROWTH AND DESALINATION. In *17th International Symposium on Ice*.

Thoms, Silke, Kutschan, Bernd, Morawetz, Klaus & Cemming, Sibylle 2014 Phase-field theory of brine channel formation in seaice: Short-time frozen structures. *Under review* pp. 1–14, arXiv: 1405.0304.

Vancoppenolle, Martin, Fichefet, Thierry & Bitz, Cecilia M. 2006 Modeling the salinity profile of undeformed Arctic sea ice. *Geophysical Research Letters* **33** (21), L21501.

Voller, V. R., Swenson, J. B. & Paola, C. 2004 An analytical solution for a Stefan problem with variable latent heat. *International Journal of Heat and Mass Transfer* **47** (24), 5387–5390.

Wells, A. J., Wettlaufer, J. S. & Orszag, S. A. 2011 Brine fluxes from growing sea ice. *Geophysical Research Letters* **38** (4), n/a–n/a.

Worster, M. G. 1992 The dynamics of mushy layers. In *Interactive Dynamics of Convection and Solidification* (ed. S. H. Davis, H. E. Huppert, U. Muller & M. G. Worster), chap. The dynami, pp. 113–138. Kluwer Academic Publishers.

Worster, M G 1997 Convection in mushy layers. *Annual Review Of Fluid Mechanics* **29**, 91–122.

universiteit hasselt

UHasselt Computational Mathematics Preprint Series

UP-16-01 *Jochen Schütz and Vadym Aizinger*, **A hierarchical scale separation approach for the hybridized discontinuous Galerkin method**, 2016

UP-16-02 *Klaus Kaiser, Jochen Schütz, Ruth Schöbel and Sebastian Noelle*, **A new stable splitting for the isentropic Euler equations**, 2016

UP-16-03 *Sergey Alyaev, Eirik Keilegavlen, Jan Martin Nordbotten, Iuliu Sorin Pop*, **Fractal structures in freezing brine**, 2016